STRUCTURAL STUDIES OF SUPPORTED BILAYERS AS CELL MEMBRANE MODEL
SYSTEMS

by

Neil T. Donovan

BS Chemistry, Pennsylvania State University, 2005

Submitted to the Graduate Faculty of

Arts and Sciences in partial fulfillment

of the requirements for the degree of

Master of Science

University of Pittsburgh

2008

UNIVERSITY OF PITTSBURGH

SCHOOL OF ARTS AND SCIENCES

This thesis was presented

by

Neil T. Donovan

It was defended on

October 19, 2007

and approved by

Sunil K. Saxena, Assistant Professor, Department of Chemistry

David W. Pratt, Professor, Department of Chemistry

Thesis Advisor: Megan M. Spence, Assistant Professor, Department of Chemistry

STRUCTURAL STUDIES OF SUPPORTED BILAYERS AS CELL MEMBRANE MODEL
SYSTEMS

Neil T. Donovan, MS Chemistry

University of Pittsburgh, 2008

The cell membrane is thought to have a much more active role in cellular function than previously known. As such, there is considerable interest in measuring the physical properties of model cell membranes to determine the biological relevance of these systems; specifically, the differences between the conventional model of a free bilayer in the form of a vesicle and a solid-supported lipid bilayer are of concern. Solid-supported lipid bilayers have been shown, using atomic force and fluorescence microscopy, to display different bulk properties than vesicles. The molecular information offered by nuclear magnetic resonance spectroscopy complements the bulk information provided by surface based techniques. We are developing NMR as a tool to probe the molecular aspects of model cell membrane structure.

A reliable method for creating supported single lipid bilayers on spherical supports has been developed by our lab. The resultant spherically supported bilayers (SSBs) have been studied using ^{2}H NMR spectroscopy to elucidate differences in structure by extracting the order parameter profile of the alkyl chains from the ^{2}H quadrupolar splitting, and by ^{1}H NMR diffusion measurements, where the diffusion coefficient is used as a spectroscopic probe of molecular behavior.

Atomic force and fluorescence microscopy studies were also done on planar supported bilayers, as a confirmation of the bilayer properties as measured by the conventional means.

Furthermore, a method was developed using AFM to indicate definitively whether or not a supported bilayer existed on the supporting mica surface.

Results indicate that there is a difference in bilayer structure between supported bilayers and the conventional model of a free bilayer. A method for extracting the alkyl chain order parameter profile is being developed, with promising initial results. Additionally, an NMR diffusion pulse sequence using the WATERGATE water suppression technique has been developed and employed on both free and supported lipid bilayers.

TABLE OF CONTENTS

LIST OF FIGURES

1.0 - INTRODUCTION

The plasma membrane of a biological cell is a complex structure consisting primarily of a phospholipid bilayer with proteins and other smaller molecules such as carbohydrates interspersed throughout. The specific lipid composition, proteins and other molecules present vary from one type of cell to another, providing a wide variety of systems. Thus, it is desirable to develop a model membrane that mimics a real cell membrane but without the unnecessary complexities. The ideal model membrane will be a single lipid bilayer that retains lateral phospholipid diffusion and exhibit coupled leaflets. An ideal model membrane will also be able to have its shape and orientation easily controlled to facilitate various spectroscopic and imaging techniques.

Two systems have emerged as useful model membranes. The conventional model consists of an onion-like structure of several concentric free-standing lipid bilayers, known as a multilamellar vesicle, or MLV. A lipid bilayer can also be deposited onto a solid support, with a thin layer of water separating the bilayer from the support[1]. This is known as a supported bilayer.

Both supported bilayers and MLVs are frequently used as model membranes for any number of applications. There are, however, some very significant differences between the two that have yet to be completely reconciled.

In an MLV, both inner and outer monolayers (called "leaflets") interact significantly with bulk water. By their very nature, however, supported bilayers have the inner leaflet interacting strongly with the solid support (Figure 1). While the MLV more closely replicates the environment of a real cell membrane, free-floating vesicles have certain disadvantages.

Specifically, free-floating MLVs are difficult to image using optical or atomic force microscopy due to motion in suspension. Furthermore, for NMR applications, the magnetic susceptibility for a phospholipid bilayer is anisotropic; the susceptibility is greater in the direction perpendicular to the plane of the bilayer[2]. This causes a free-floating spherical MLV to deform and take on an elliptical shape when placed in a strong magnetic field.

The phase behavior of supported lipid bilayers is different than that of vesicles. Phospholipids display an order-disorder phase transition (called "chain melting," also colloquially referred to as the "main phase transition"), and this transition, T_m, is sensitive to the lipid surroundings. Through differential scanning calorimetry, it has been shown that the main phase transition for pure DMPC vesicles is very sharp, occurring over a temperature change of 0.1 °C[3]. For a pure DMPC supported bilayer, though, Tokumasu et al. have shown the main phase transition temperature to be increased by roughly 5 °C and significantly broadened to almost 8 °C[4]. Charrier and Thibaudau have shown that, for a pure DMPC mica-supported bilayer, there are two transitions that occur, which are attributed to independent melting of the top and bottom leaflets[5]. This hypothesis is supported by DSC studies of supported bilayers on small chips of mica[6]. The surface-bottom leaflet interaction is suspected to be the cause of this behavior, and it is not yet known if the extent of leaflet decoupling can be controlled.
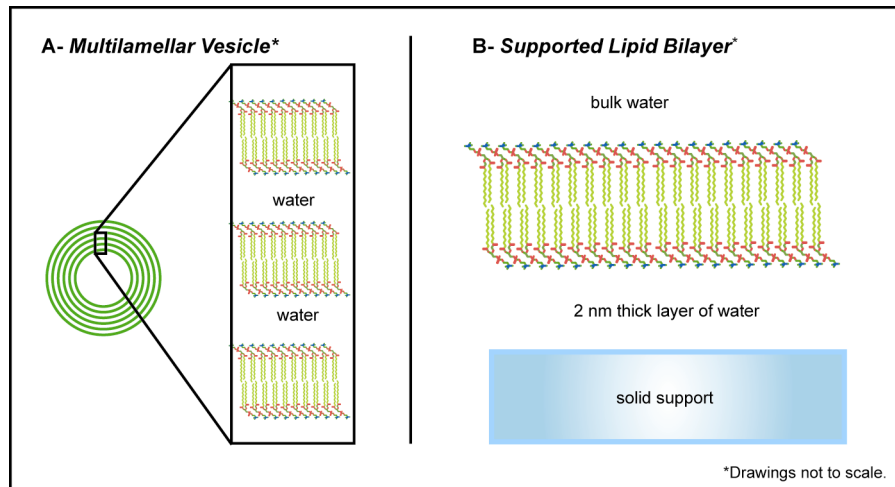
Figure 1: Illustration of the differences between MLV and supported bilayer systems. Courtesy
M. M. Spence

1.1 - LIPID RAFTS IN MLVs AND SUPPORTED BILAYERS

Lipid rafts[7] behave differently in MLVs as opposed to supported bilayers. Using fluorescence microscopy, it has been shown that lipid rafts move freely around the surface of free-floating vesicles[8-11]. If the vesicle suspension is heated such that all of the rafts melt and is then cooled again, lipid rafts reform (albeit in completely random locations). However, in a supported bilayer, lipid rafts are stationary on the scale of hours (Figure 2). Upon heating, the lipid rafts vanish as expected, but do not reform upon cooling[8]. It has been shown that this hysteresis behavior can be eliminated by altering the surface chemistry of the support[12], indicating that perhaps other properties of supported bilayers can be manipulated in the same manner as well.
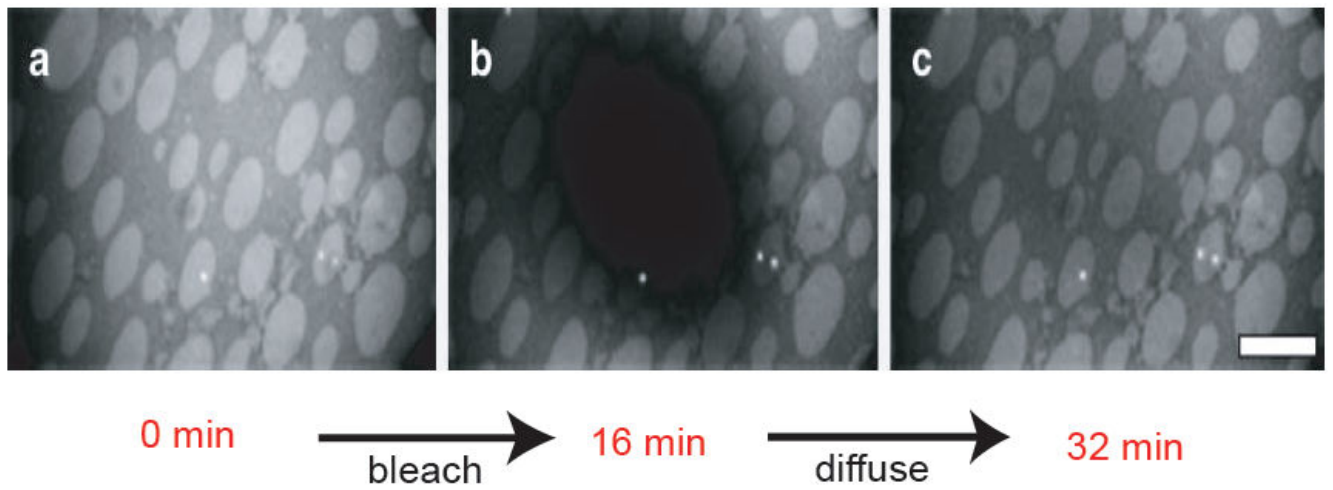
Figure 2: Fluorescence Recovery After Photobleaching (FRAP) image illustrating the immobility of lipid rafts (lighter regions) in a supported bilayer. Taken from Reference 8.

2.0 - MATERIALS AND METHODS

2.1 - INSTRUMENTAL DETAILS

2.1.1 - NMR SPECTROSCOPY

All NMR measurements were carried out using an 11.7 T magnet (^{1}H ω_0 / 2π = 500 MHz) equipped with a Bruker Avance 500 console, BCU05 Variable Temperature Control Unit, and using Bruker Topspin 1.3 software. All sample rotors were Bruker 4 mm ZrO_2 MAS rotors. The internal rotor volumes were 12 µL, 50 µL, or 200 µL. ^{2}H NMR experiments were carried out at 305 K (unless explicitly stated otherwise) using a Bruker HXY broadband MAS probehead tuned to 76.8 MHz. ^{2}H RF field strength was 78 kHz (3.2 µs 90º pulse width), and a minimum of 8192 scans were collected, each consisting of 2048 complex data points. ^{2}H spectra were acquired using a quadrupolar echo pulse sequence, with 50 µs between pulses. The acquisition time was 10 ms, spectral width was 100 kHz, and the recycle delay was 250 ms. The sample volume used was 200 µL, and the rotor was not spun for these experiments. All ^{1}H experiments were carried out using a Bruker hr-MAS probehead of ^{1}H - ^{13}C - ^{15}N - ^{2}H lock configuration, equipped with a z-gradient coil capable of 0.513 T/m gradient strength at 10 A. ^{1}H RF field strength was 53 kHz (4.7 µs 90º pulse width). 64 scans were collected for MLV samples, and a minimum of 128 scans were collected for SSB samples. Spectral width was 5 kHz, unless explicitly stated otherwise. MLV samples were kept in a 12 µL MAS rotor, and SSB samples used a 50 µL MAS rotor for acquisition. The MAS rate for all ^{1}H experiments was 5 kHz. WATERGATE water suppression techniques were used to remove residual ^{1}H$_2$O signal.

2.1.2 - ATOMIC FORCE MICROSCOPY

All AFM measurements were carried out in tapping mode using a Veeco/Digital Instruments atomic force microscope with NanoScope III controller and type G scan head (98 μm maximum lateral displacement). AFM tips used were MikroMasch NSC21 type with Al coated back sides; the longer cantilever (k = 1 N/m) was used for all experiments. The cantilever was driven at about 8 kHz (adjusted for maximum amplitude for each experiment), and the imaging force did not exceed 10 nN. Scan sizes ranged from 500 nm to 5 μm, and the scan rate was always 1 Hz. For each experiment, 256 points were collected in each of 256 lines, unless stated otherwise.

2.1.3 - SUBSTRATE PREPARATION

For mica-supported bilayers, freshly cleaved mica of the highest grade was used (PELCO mica discs, Ted Pella, Inc.). Glass supports were treated by boiling 20 min in 2% ICN 7X detergent, followed by immersion in warm (~40 ºC) 2% HNO_3 for 20 min. Lastly, glass supports were plasma etched for 10 min in an O_2 plasma. Glass supports were used within 10 min of plasma etching.

2.1.4 - FLUORESCENCE MICROSCOPY

All fluorescence microscopy experiments were carried out using an Olympus BX51 microscope with epifluorescence attachment. The source was a 100 W Hg-arc lamp filtered through the appropriate filter sets for the fluorophore of choice. An Olympus LUMPLFL/IR2 40x water immersion objective (NA = 0.80) was used for all experiments, and images were captured using a Hamamatsu C9100 digital camera equipped with a 2x magnifying lens. The filter set was chosen to permit excitation light of 488 nm to reach the sample, while allowing emission of 605 nm to reach the detector. During photobleaching, the focal stop was used to reduce illumination to a spot 350 μm in diameter. Maximum intensity excitation light was used to bleach for a

minimum of 20 s, following which, the excitation light was attenuated by a minimum factor of 1000 for observation. Furthermore, the lamphouse shutter was only open during active viewing to minimize additional bleaching.

2.2 - PREPARATION AND CHARACTERIZATION OF SUVs

One of the most widely used lipids for model membrane study is dimystyroyl-*sn*-glycerophosphatidylcholine, DMPC, the structure of which is shown below in Figure 3. DMPC is often used because its chain melting phase transition temperature occurs near room temperature (23.7 ºC at ambient pressure, measured by differential scanning calorimetry)[3]. DMPC-d_{54}, which has the alkyl chains fully deuterated, was used for all ^{2}H NMR experiments. The procedures for using DMPC-d_{54} are identical to those of the undeuterated compound, with the sole exception that ^{2}H-depleted water was used in place of D_2O.

Small, unilamellar vesicles were prepared in the manner described by Barenholz, et al.[13]. To wit, either D_2O (for most experiments, supplied by Cambridge Isotope Laboratories) or ^{2}H depleted water (for ^{2}H NMR spectroscopy only, 2-3 ppm ^{2}H, supplied by Cambridge Isotope Laboratories) was added to powdered DMPC (Avanti Polar Lipids) to achieve 3 mg/mL concentration. The mixture was vigorously vortexed until uniform in appearance. The resultant opaque liquid was then probe sonicated for 30 minutes or until clear, whichever was longer. The sonication power used was 5 W, and during sonication, the mixture was cooled by immersion in a cool water bath. Following sonication, the suspension was transparent with a slight blue color. This suspension was then filtered through a 0.22 µm Millipore filter.

Previous work done by Jen Kulzer and Shanna Price, undergraduates in the Spence research group, has shown that this method consistently produces SUVs with a narrow size

distribution centered about 25 nm radius, as characterized by dynamic light scattering. Vesicles prepared in this manner are stable for weeks at 4 ºC, though for all experiments described herein, vesicles were always freshly prepared (within 3 days of use).

The final DMPC concentration in the vesicle suspension was measured using a colorimetric method[14]. Briefly, 2.7 g $FeCl_3 \cdot 6 H_2O$ (10 mmol, Aldrich) and 3.0 g NH_4SCN (40 mmol, Aldrich) were combined in 100 mL H_2O to yield a dark red, almost black solution. This solution (hereafter referred to as "SCN reagent") is stable for months at room temperature if kept in an amber bottle. A 2 mg/mL solution of DMPC in CH_2Cl_2 (J. T. Baker) was used to dispense 100 µg aliquots of DMPC for use as standards (100 µg – 500 µg, in 100 µg increments), and 100 µL of vesicle suspension was used as the test sample. After all CH_2Cl_2 had evaporated from the calibration samples, 1 mL SCN reagent was added to all samples, followed by 4 mL CH_2Cl_2. The SCN reagent was added first to minimize evaporation loss of the highly volatile (bp 41 ºC) CH_2Cl_2. The samples were then capped and gently vortexed until the ruddy color was uniform throughout the bottom (organic) layer, which usually took about 1 min, after which the samples were allowed to sit undisturbed for 20 min. The bottom layer was drawn off, and its absorbance at 488 nm was measured immediately, using an HP 8453 UV-Vis spectrophotometer with a tungsten filament source.

The SCN reagent forms a complex with the phosphate head group of the lipid, which is preferentially soluble in CH_2Cl_2. Thus, the CH_2Cl_2 takes on a slight red color that increases in intensity with increasing phospholipid concentration. The excitation wavelength of 488 nm was chosen since it is the wavelength of maximum absorbance for the complex.

All vesicles used for the experiments described herein were freshly prepared and characterized (within 3 days of use) to ensure quality. Vesicles were stored at 4 ºC when not in use.
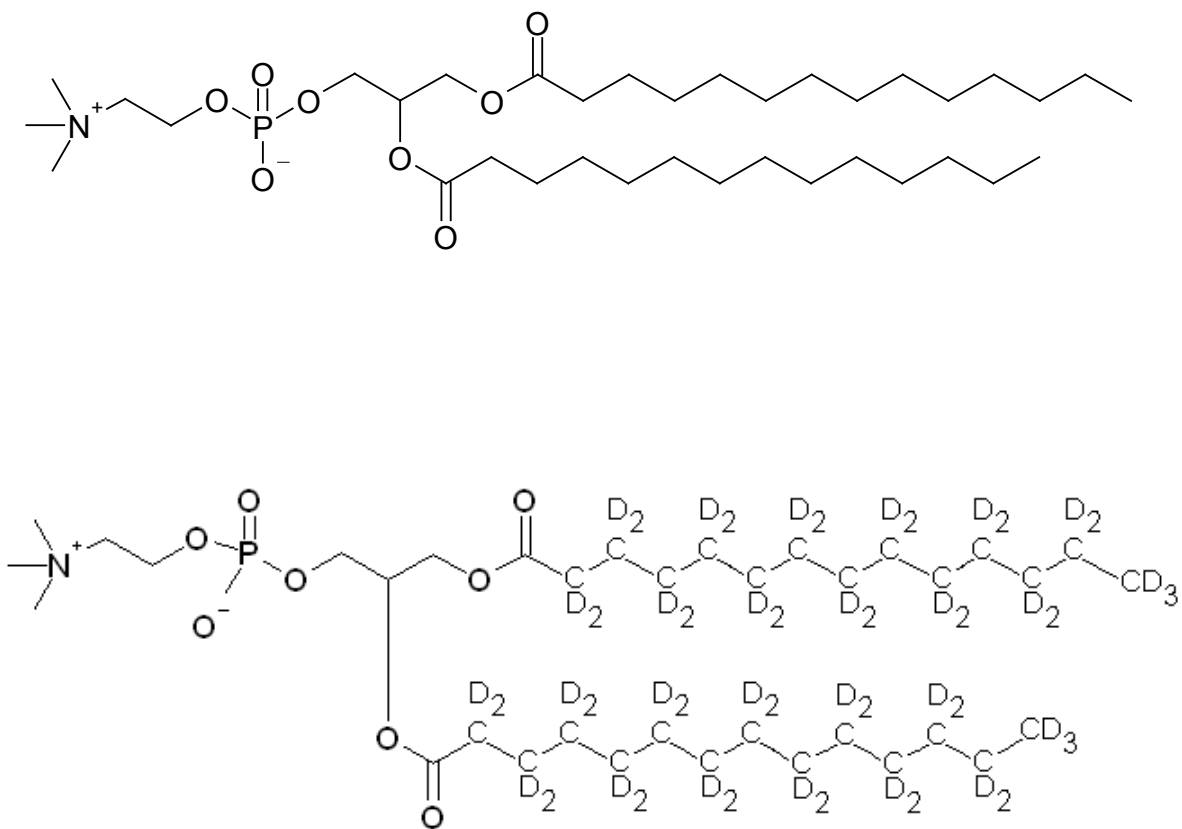
Figure 3: Structures of DMPC (top) and DMPC-d_{54} (bottom).

2.3 - CREATION OF SUPPORTED BILAYERS

The SUVs are then exposed to a smooth surface such as mica or silica, onto which they adsorb intact (albeit slightly deformed). Once a critical concentration of adsorbed vesicles is achieved, the vesicles spontaneously rupture, laying down a patch of bilayer[15]. This adsorption and rupture process can continue until the surface is completely covered. This "supported bilayer" as it is called is separated from the solid surface by a thin layer of water which is roughly 2 nm thick[16,17] and is stable for weeks. However, the supported bilayer must be kept under water or a suitable buffer at all times, as the supported bilayer desorbs if exposed to air[18]. The cartoon[19] in Figure 4 roughly illustrates the deposition process.

For NMR studies, supported bilayers were created on spherical substrates[16] consisting of silica microspheres 0.97 μm in diameter. Spherical substrates were chosen over the conventional choice of planar substrates due to the higher packing efficiency of spheres over planes. Many more supported bilayers could be packed into the limited volume of an MAS rotor (total volume 50 μL) than could be achieved using stacked glass plates and a goniometer stage assembly[20]. The impacts of using a spherical support rather than a planar one are easily accounted for and will be discussed in detail later. The surface smoothness and size of the spherical supports were measured by the manufacturer using SEM and dynamic light scattering. The microspheres were stored in either D_2O (for most experiments) or ^2H depleted water (for ^2H NMR experiments only) at 4 ºC when not in use, as per the manufacturer's recommendation. The concentration of microspheres was $1.129 \cdot 10^{11}$ / mL for all stock suspensions. Apart from changing the solvent, the microspheres were used as supplied.

Spherical supported bilayers (SSBs) were created in the manner described by Bayerl and Bloom[16]. To wit, 456 μL of microsphere suspension was combined with the desired amount of

vesicle suspension (the exact amount is discussed in detail later). The sample tube was then vortexed vigorously for 1 min., followed by centrifugation at 2000g for 30 s or until all of the microspheres had pelleted out. The liquid above the pellet was decanted off, and 500 µL D$_2$O (or ^{2}H depleted water for ^{2}H experiments) was added. The pellet was then dispersed by vigorous vortexing. This vortex-centrifuge-decant-add clean solvent cycle was repeated 5 times to ensure that any vesicles that did not adsorb were removed. Following the final wash, the pellet, which had the consistency of paste, was scooped up with a stainless steel spatula and pushed into an MAS rotor, using a plastic powder-packing tool and needle to remove any air bubbles present. This procedure yields sufficient material to fill a 50 µL MAS rotor, and can be scaled appropriately for different rotor sizes.
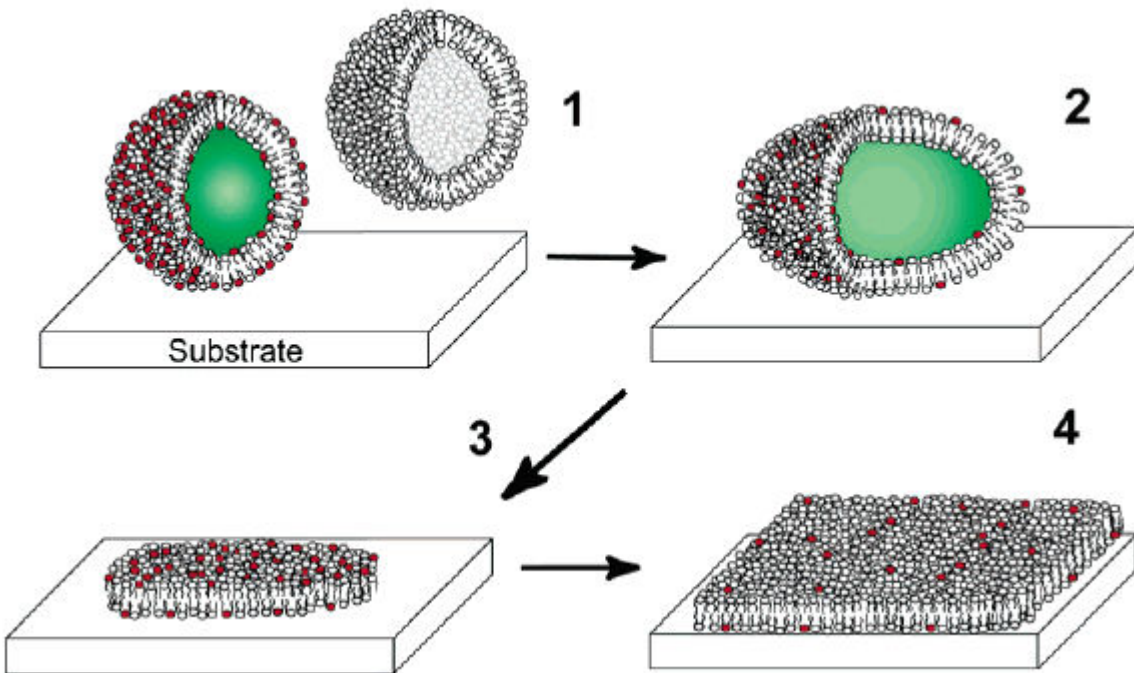
Figure 4: Cartoon representation of the vesicle fusion process. Vesicles adsorb intact and deform. Once a critical concentration is reached, the vesicles rupture and deposit a patch of supported bilayer. This process repeats until the surface is covered. Drawing taken from Ref. 19.

3.0 - RESULTS

3.1 - ^{1}H NMR COVERAGE TITRATION – CONFIRMATION OF SINGLE BILAYER STATUS

To confirm that supported bilayer formation is self-limited after one bilayer is deposited, increasing amounts of vesicles were added to a fixed number of microspheres, and the resultant SSBs were analyzed by ^{1}H NMR. If there is no limit to the number of bilayers that can be deposited, then the ^{1}H NMR signal intensity should increase with increasing amount of vesicles added; the signal intensity leveling off is a sign that bilayer deposition is self-limited.

The "stoichiometric" amounts of vesicles to add were calculated as follows:

Amount of microsphere suspension added:	456 μL
Microsphere concentration:	$1.129 \cdot 10^{11}$ / mL
Total number of microspheres added:	$5.14 \cdot 10^{10}$
Microsphere diameter:	0.97 μm
Total surface area of all microspheres:	0.152 m^2
Area occupied by one DMPC headgroup[16]:	55 Å^2
Total number of headgroups needed to cover all microspheres:	$2.8 \cdot 10^{17}$

Remembering that a bilayer is two molecules thick, this means that **$5.6 \cdot 10^{17}$** DMPC molecules are required to cover all of the microspheres with a supported bilayer. This amount is hereafter referred to as one "equivalent."

15

Considering that the DMPC concentration is different from one vesicle preparation to the next, the following convenient relation between vesicle concentration and amount to add was calculated.

$$\frac{623}{\left[{mg}\middle/{mL} \right]} = amt. \, in \, \mu L \, for \, 1 \, equivalent$$

With that said, increasing numbers of equivalents were added to the same number of microspheres in a titration experiment. The observable was the ^{1}H signal intensity, particularly from the alkyl chain methylenes and methyls, and the choline group methyls (strongest intensities).

Blank microspheres were run to determine what background signals would be present, along with one, five, and ten equivalents added. The spectrum is presented as Figure 5. Additionally, samples were prepared with two and three equivalents added; the signal intensity was observed to increase up to 5 equivalents added (data not shown).

The fact that adding one equivalent does not provide complete coverage is not unexpected. As stated above, in the vesicle fusion process, the vesicles adsorb intact. Once a critical concentration of vesicles is achieved, the vesicles rupture to form a supported bilayer, ejecting some bilayer material back into solution (the QCM traces in Ref. 15 show that the amount of adsorbed material increases and then sharply decreases to the expected value for a single supported bilayer; the remainder is ejected into solution and cannot be used to form supported bilayers).

Conclusion: 5 equivalents of vesicles should be used when preparing SSBs to ensure maximum coverage.
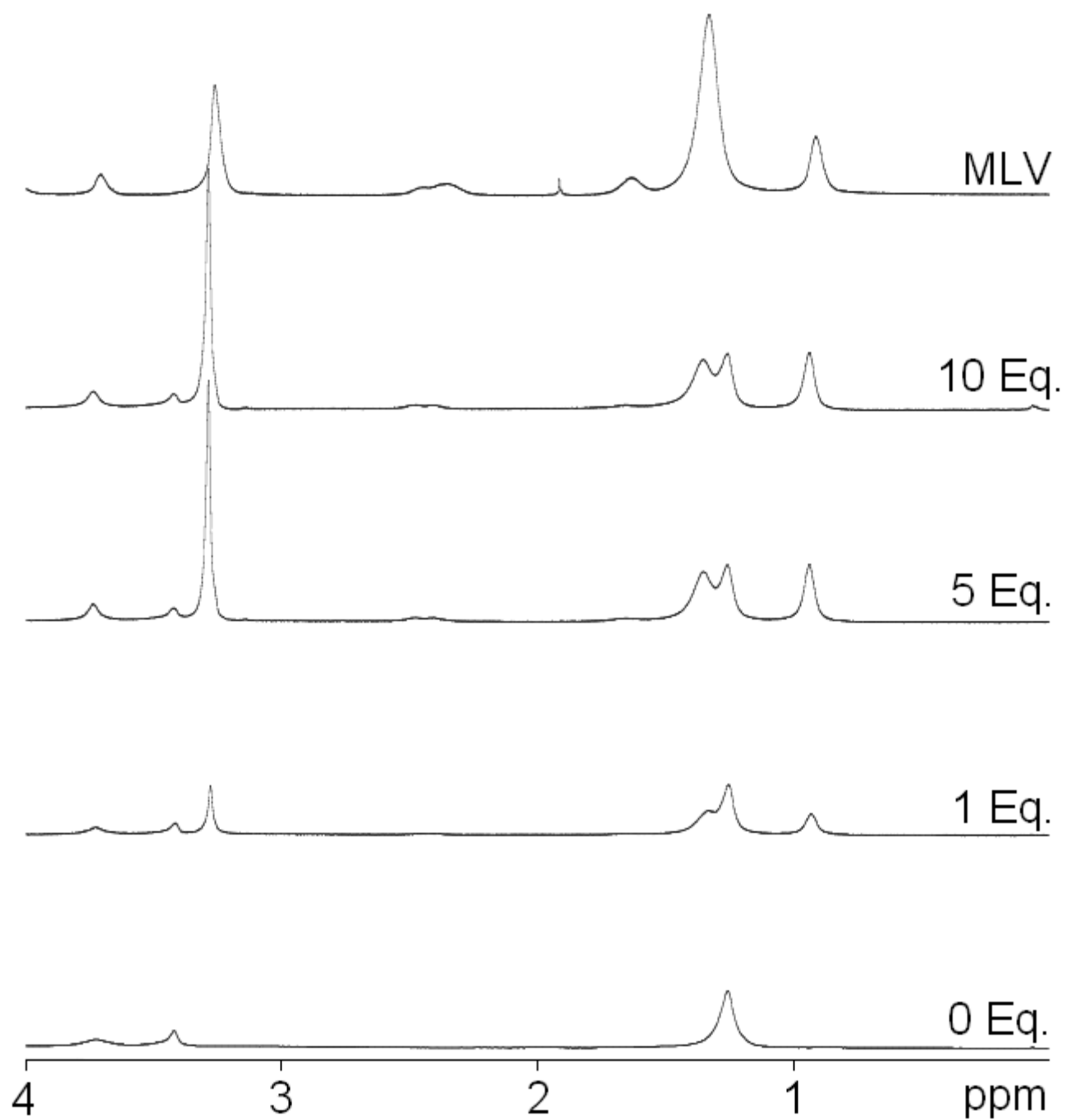
Figure 5: ^{1}H NMR spectra of SSBs made with increasing number of equivalents. The top spectrum is provided as a reference and is not on the same scale as the rest.

3.2 - BILAYER PRESENCE TEST FOR SUPPORTED BILAYERS

In addition to making supported bilayers on a spherical surface, it is also possible to make them on a planar surface. This enables the use of, among other techniques, AFM for imaging. The process for depositing a supported bilayer onto a planar surface is not very different from the spherical surface preparation mentioned previously. Briefly, a drop of vesicle suspension is placed onto the clean, flat support surface (either freshly cleaved mica or plasma-etched glass) and allowed to sit for 60 s. The planar surface is then moved to a dish of clean water or buffer and shaken vigorously for 30 s to dislodge any unadsorbed material (this is analogous to the vortex-centrifuge-add clean solvent procedure mentioned for the SSB preparation).

A test was devised to determine whether or not a supported bilayer was present on a glass substrate, as both a blank surface and a planar supported bilayer appear on the AFM as vast flat expanses. The AFM tip was moved up and down above the surface, and the surface-tip interaction was measured by monitoring the oscillation amplitude of the cantilever as a function of vertical distance. It was found that, for a blank glass surface, once the tip was in contact with the surface and then pulled away, a residual force held the tip on the surface. This manifests itself as a hysteresis loop in the force plot. This hysteresis is not present for a surface with a supported bilayer. The force plots illustrating this are shown below as Figure 6. While this method has not yet been tested for a mica-supported bilayer, it is expected that the effect would be similar or even more pronounced, as the mica surface charge density of mica is greater than that of glass, and both freshly cleaved mica and plasma-etched glass are completely hydrophilic.

A

Extending
Retracting

Amplitude
2.50 nm/div

Setpoint

0.00   Z - 2.50 nm/div   50.00

B

Extending
Retracting

Amplitude
2.50 nm/div

Setpoint

0.00   Z - 5.00 nm/div   100.00

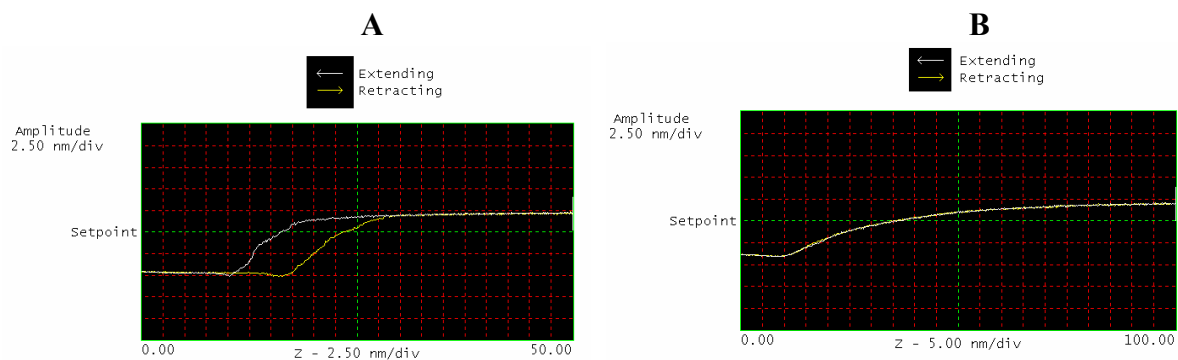Figure 6: **(A)** AFM force plot for a blank plasma-etched glass surface. **(B)** AFM force plot for a plasma-etched glass-supported bilayer. The y-axis corresponds to the tapping-mode amplitude of the AFM cantilever, and the x-axis is vertical distance from the surface. The white line is the trace when the tip is moving down (toward the surface), and the yellow line is when the tip is being pulled away from the surface.

3.3 - [2]H SPHERICAL SUPPORTED BILAYERS – OBTAINING AN ORDER PARAMETER PROFILE

The ^{2}H NMR spectrum of a deuterated lipid membrane displays the structure and dynamics of each lipid segment. The ^{2}H NMR spectrum for a DMPC-d$_{54}$ SSB is presented as Figure 7. Additionally, a ^{2}H NMR spectrum of DMPC-d$_{54}$ MLVs was taken for comparison purposes; it is presented as Figure 8.

In the ^{2}H spectra presented, the dominant spectral feature is the ^{2}H quadrupole coupling interaction. The magnitude of the quadrupole coupling is related to the spacing between the superposed doublets. However, for both the SSB and MLV samples, the ^{2}H NMR spectrum is complicated by the fact that the frequency depends on orientation, and that the spectrum for each segment is superposed to yield the total pattern. The rapid rotation of phospholipid molecules about the bilayer normal (essentially spinning in place, Figure 9)[2] reduces the angular dependence of the quadrupolar coupling to the angle, θ, between the bilayer normal and the static field. This rapid rotation simplifies the expression for quadrupolar splitting. The expression for the quadrupole splitting[2,16,21-23] in this case is given by

$$\omega = \omega_Q S_{CD} P_2(\cos\theta) \cdot p(\theta)$$

where ω_Q is the ^{2}H quadrupolar coupling constant, θ is the angle between the static field and the axis of molecular rotation, and $P_2(\cos\theta)$ is the second Legendre polynomial, $P_2(\cos\theta) = \dfrac{3\cos^2\theta - 1}{2}$. Additionally, the ^{2}H NMR spectrum is also influenced by the angular distribution of phospholipid molecules, determined by the geometry of the membrane. For an SSB, the rigid support makes the angular distribution function that of a sphere, $p(\theta) = \sin\theta$. Thus, while molecules at the poles of the sphere have the largest quadrupole splitting ($P_2(\cos 0)$

$= P_2(\cos \pi) = 1$), their contribution to the Pake pattern is zero ($\sin(0) = \sin(\pi) = 0$); this simply

represents that there are many, many more molecules at the "equator" than at the poles.
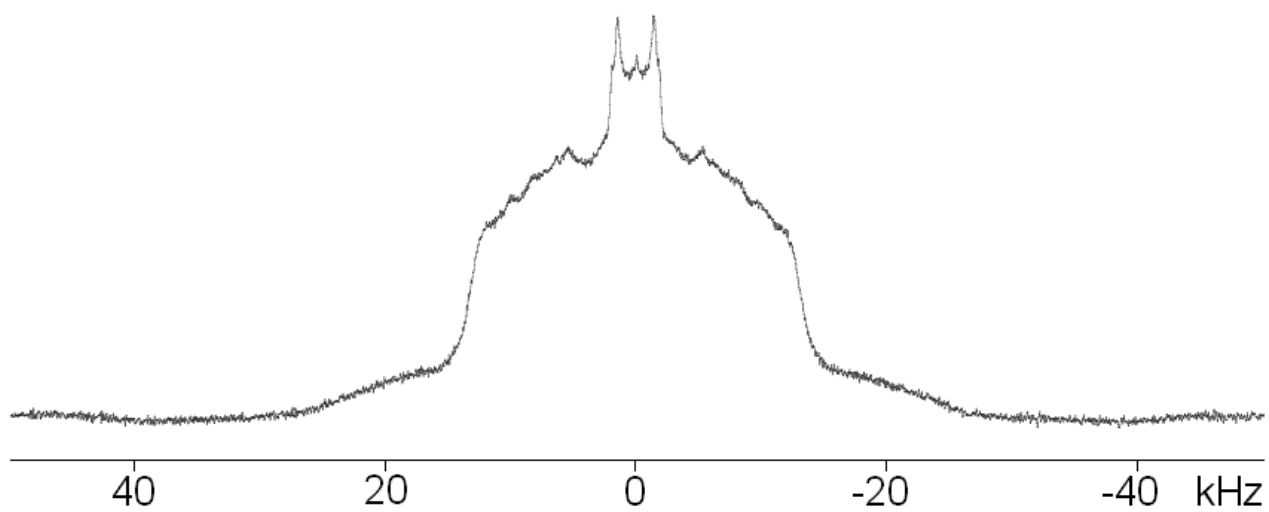
Figure 7: ^{2}H NMR spectrum of DMPC-d$_{54}$ SSBs. 102400 scans collected at 32 ºC.
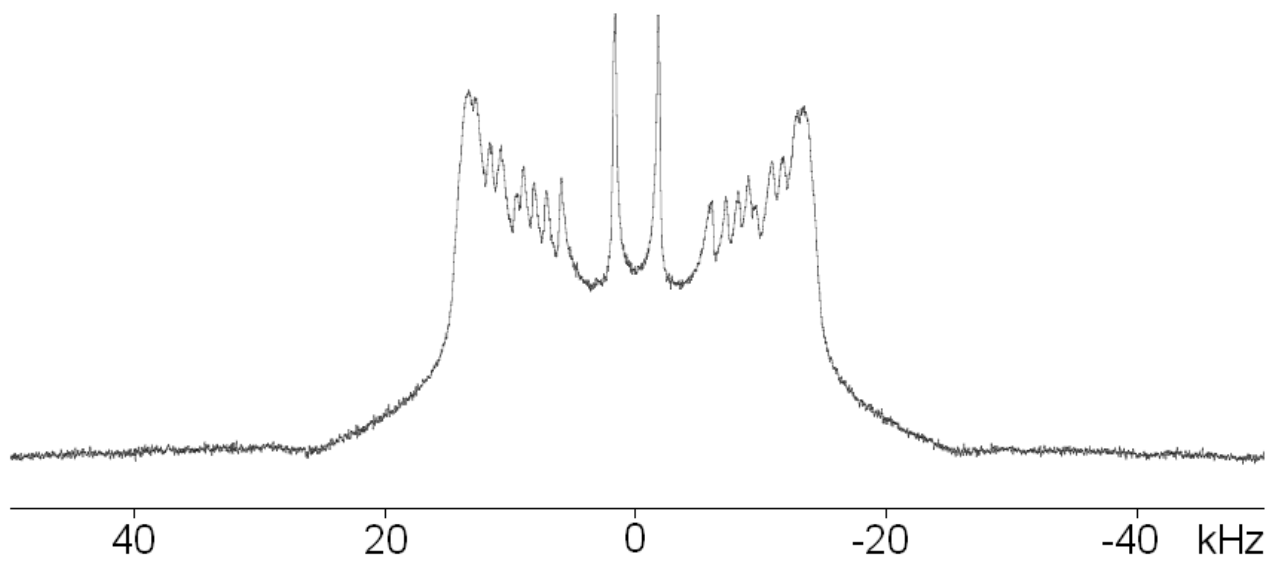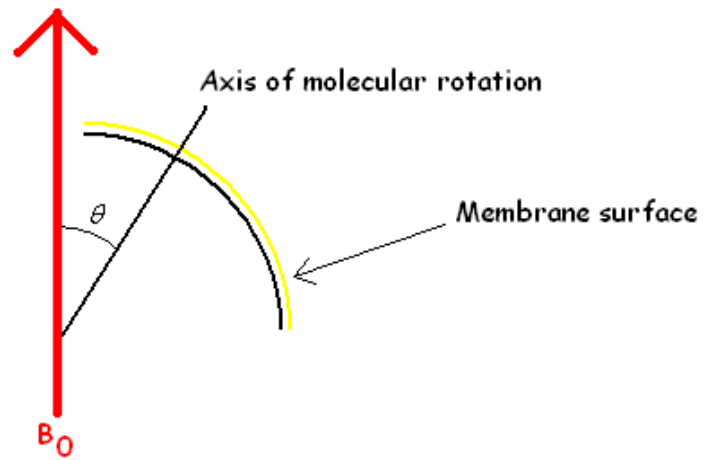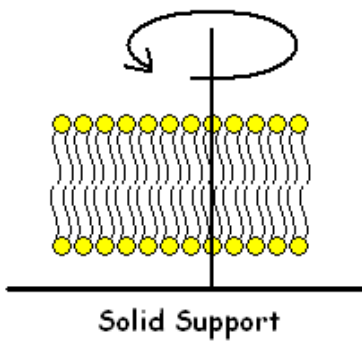
Figure 8: ^{2}H NMR spectrum of DMPC-d_{54} MLVs. 8192 scans collected at 32 ºC.

Figure 9: **Left**: Illustration of rapid phospholipid rotation about the bilayer normal. **Right**: Illustration showing the relation of θ to B_0.

3.3.1 - EXTRACTION OF THE ORDER PARAMETER

The order parameter profile is usually constructed by mathematically deconvoluting the ^{2}H NMR spectrum in a process called dePakeing[23]. This method effectively turns a powder spectrum into a spectrum of a single crystal of the same material by removing all angular dependence; thus, any residual splitting present must be from the S_{CD} term. The process of dePakeing is computationally very intensive, and is often done on supercomputing clusters (Sternin et al. have developed a method to extract both the probability distribution function *and* the order parameter simultaneously, for use on magnetically deformed MLVs[2,24]). However, since for the SSB system, the orientational distribution function is known, a simpler approach can be taken. To that end, a model is being developed that collects "Pake doublets" of varying order parameters (from a discrete list) and adds them together to reproduce a ^{2}H NMR spectrum. By comparing the simulated and real spectra and minimizing the misfit between them, the order parameter profile can be obtained without the need for a supercomputer. The model consists of a doublet lineshape function whose splitting is modulated by angle and order parameter. In this simple case, the only parameter that needs to be entered manually is the linewidth (for simplicity, all peaks in the Pake pattern have the same linewidth, although that could easily be remedied in a later version of the model). The model function for one individual doublet is as such[25], where λ is the linewidth parameter, and the other symbols have the usual meanings:

$$A(\omega,\lambda,\theta,S_{CD}) = \left[\frac{\lambda}{\lambda^2 + \left(\omega + \frac{1}{2}S_{CD} \cdot (3\cos^2\theta - 1)\right)^2} + \frac{\lambda}{\lambda^2 + \left(\omega - \frac{1}{2}S_{CD} \cdot (3\cos^2\theta - 1)\right)^2} \right] \sin\theta$$

So, to obtain a spectrum for a group of superposed doublets, a list of values for S can be used, while integrating over all relevant values of θ (i.e., 0 to π). Some "sample spectra" are shown as Figures 10-13.
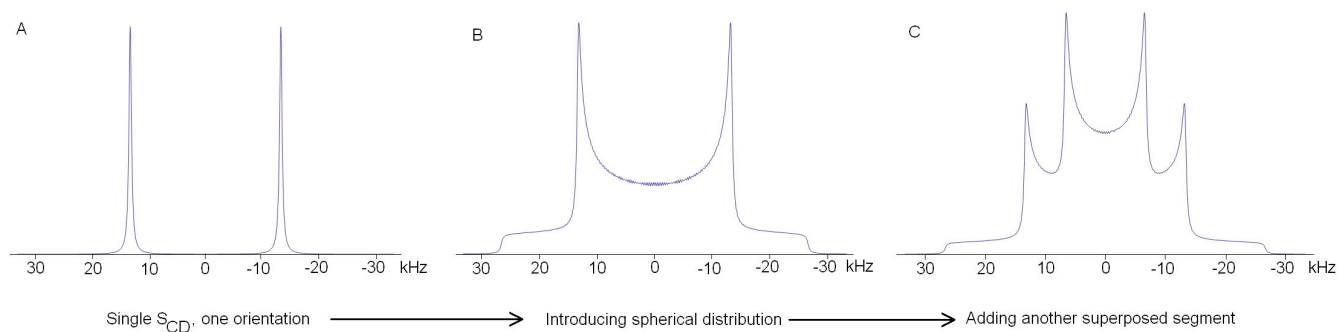
Figure 10: Illustration of the "building-up" of a simulated ^{2}H NMR spectrum. **(A)** is the simulated ^{2}H NMR spectrum of a single value of S_{CD} with only one orientation; **(B)** still only has one value of S_{CD} but introduces a spherical distribution; **(C)** now adds in a second value of S_{CD}, showing the superposition of the two patterns.
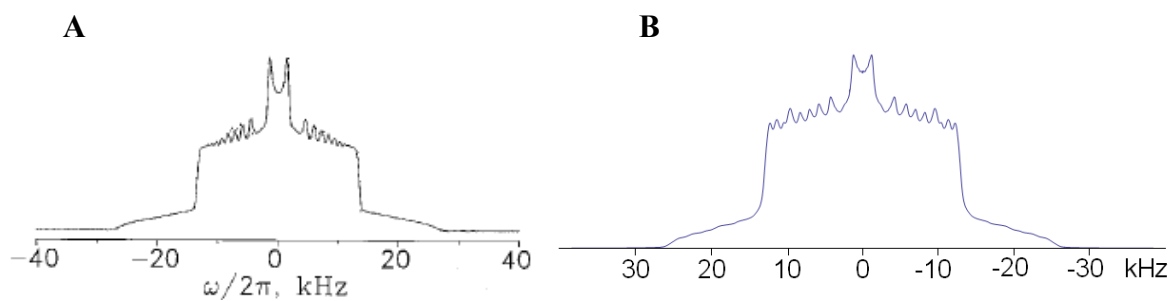
Figure 11: Side-by-side comparison of simulated and actual ^{2}H NMR spectra. **(A)** is an actual ^{2}H NMR spectrum for a spherical distribution of POPC (Ref. 2) **(B)** is a simulation of that same spectrum obtained by measuring the peak splitting and obtaining an order parameter profile
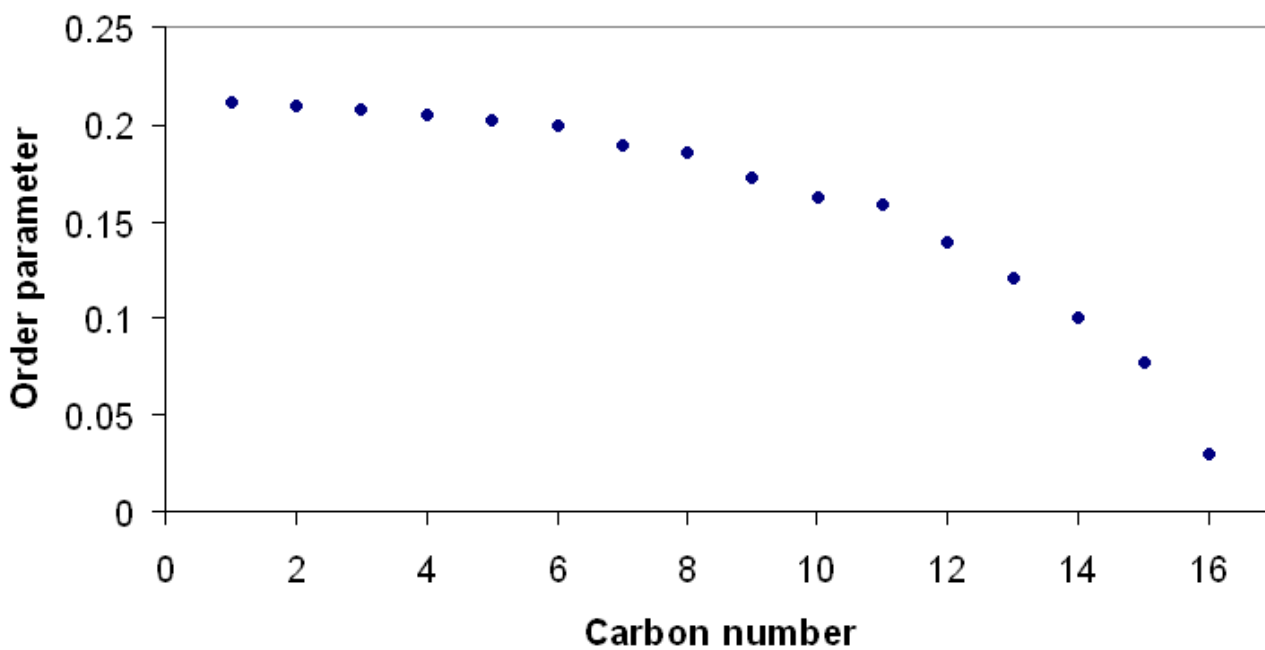
Figure 12: Order parameter profile for the simulated spectrum in Figure 11. This calculation is in good agreement with the published values.
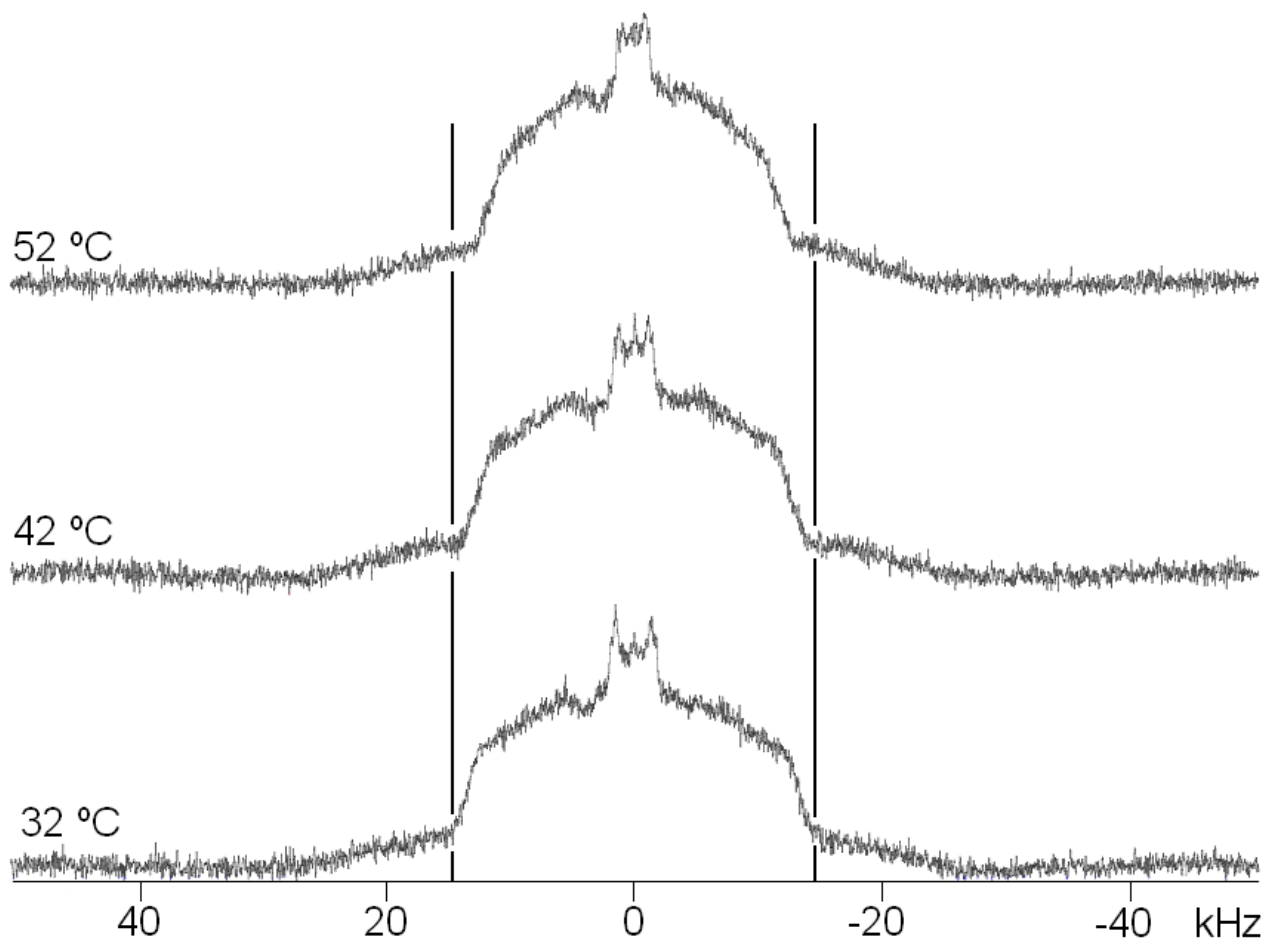
Figure 13: Actual ^{2}H NMR spectra of DMPC-d_{54} SSBs at varying temperatures. 8192 scans each; the vertical bars indicate the edges of the widest pattern and are added to help show how the patterns narrow with increasing temperature.

As can be seen from the comparison in Figures 11 and 12, the model has potential for easily extracting an order parameter profile from a ^{2}H-SSB NMR spectrum. The simulated spectrum on the right in Fig. 11 was developed very quickly using only the human eye as a gauge; a least-squares fitting is the next logical step. The simulation used here, though, would likely be inadequate for use with a system in which both S_{CD} and $p(\theta)$ were unknown, as that calculation would require substantially more computing power[2,24].

3.3.2 FUTURE ^{2}H NMR EXPERIMENTS

Firstly, the already-obtained ^{2}H NMR spectra should be properly fitted using the simulation, and the order parameter profile obtained should be compared to published values. Once this straightforward task is completed, the next step would be the addition of secondary components to the lipid mixture and concomitant ^{2}H NMR analysis. The use of secondary components would enable the formation of lipid rafts, from which order parameter profiles could be extracted. In addition to yielding insight as to basic phase behavior (measured by taking several spectra at varying temperatures), it is expected that two populations will be observed in the order parameter profile for a lipid raft-containing SSB, and the ^{2}H NMR spectrum could also quantify how much of each phase is present.

3.4 - LIPID DIFFUSION AS MEASURED BY ^{1}H NMR

Phospholipids in a plasma membrane are not static, but rather are free to move in the plane of the bilayer on the timescale of μs to ms[8-11,26-28]. This motion is restricted to in-plane movement only; the timescale for lipid molecules flipping from one leaflet to the other is on the order of seconds to minutes[20]. This motion can be detected by labeling the bilayer (either free-standing or supported) with a fluorescent tag, photobleaching a selected region, then observing the

fluorescence intensity return. This is known as "fluorescence recovery after photobleaching," or FRAP, and is a common technique in fluorescence microscopy. This method, though, requires the addition of fluorophores, which often have large, charged groups present that may alter the behavior of the membrane under study. Indeed, it has been shown that, depending on the charge of the fluorophore, tagged supported bilayers can behave very differently from untagged ones[29]. Thus, it is desirable to use a method that requires no external labeling agent; diffusion measured by NMR meets this condition.

3.4.1 PRINCIPLES AND METHODS

It has been known for some time that an NMR signal can be modulated in a characteristic way by applying a carefully timed series of RF pulses[30]. Diffusion can be detected by applying magnetic field gradient pulses at known times; if molecular motion occurs, the gradient pulses cause the transverse magnetization to refocus incompletely, resulting in a decrease in signal intensity[31]. A common experiment that employs this technique is the stimulated echo (known hereafter as STE). The STE experiment is used preferentially over the simpler Hahn echo solely due to the fact that the Hahn echo stores the magnetization as transverse for the duration of the experiment, whereas the STE experiment stores the magnetization longitudinally. Often, the diffusion time is very long (100 ms – 1 s), so this is necessary to prevent the signal from decaying due to faster transverse relaxation before it can be observed. The "standard" STE with pulsed field gradients (PFG-STE) works very well for two-dimensional motion, that is, if the lipids are constrained to move in a plane[31], as in a planar supported bilayer. When diffusion occurs on a curved surface such as for an SSB or MLV, though, the anisotropic magnetic susceptibility[2] of the bilayer causes inhomogeneous signal attenuation by creating a "background gradient[32]." This causes the diffusion coefficient to appear to be much larger than it actually is. This problem of background

gradients can be remedied by breaking the gradient pulse into separate parts with π pulses in between to refocus any dephasing caused by the background gradients, such as for a CPMG experiment[33]. This modified STE sequence with separated gradients and water suppression is shown schematically in Figure 14.

3.4.2 NMR DIFFUSION EXPERIMENTS

As a proof-of-concept, this pulse sequence has been applied to a single-component, single-phase MLV sample, and a bulk diffusion coefficient has been extracted following the published methodology[20,31,32,34-37]. Briefly, by measuring the signal attenuation as a function of gradient strength, the diffusion coefficient can be obtained using a modified Stejskal-Tanner equation[37]:

$$\ln(S) = -(\gamma \cdot g \cdot \delta)^2 \cdot D \cdot \left(\Delta - \frac{T}{2} - \frac{\delta}{6}\right)$$

Here, γ is the gyromagnetic ratio for the nucleus under study, g is the gradient strength, δ is the duration of the gradient pulse, D is the diffusion coefficient, Δ is the time between the first and second sets of gradient pulses, and T is half the duration that the magnetization is transverse. These relationships are illustrated in Figure 14. This equation is usually simplified to the form

$$\ln(S) = -k \cdot D$$

where k is defined as

$$k \equiv (\gamma \cdot g \cdot \delta)^2 \cdot \left(\Delta - \frac{T}{2} - \frac{\delta}{6}\right)$$

As a test of this newly written pulse program, following the methodology of Gaede and Gawrisch[34], a series of NMR diffusion experiments were conducted on unlabeled DMPC MLVs. For this series, d = 5 ms, D = 150 ms, and g was incremented from 2.6 G/cm to 48.7 G/cm in steps of 3 G/cm (5% - 95% gradient strength). The signal attenuation plot and selections of representative spectra are shown in Figure 15.

The diffusion coefficient measured for this MLV sample is $2 \cdot 10^{-12}$ m^2/s. This value is on the same order of magnitude as published values ($D = 6.5 \cdot 10^{-12}$ m^2/s is the published value, measured by FRAP. However, there are several published values that vary by approximately a factor of two for the same system, using different measurement methods.).

3.4.3 FUTURE NMR DIFFUSION EXPERIMENTS

NMR diffusion studies could provide confirmation of the decoupled leaflet melting phenomenon; in the temperature region where the top leaflet has melted but the bottom has not, it is expected that two populations with different diffusion coefficients would be observed. This hypothesis is supported by the fact that it has been confirmed that the diffusion coefficient in a supported lipid bilayer is characteristic of phase[20,35,36]. Furthermore, since the diffusion coefficient is characteristic of phase, and lipid rafts are in the l_o phase and the bulk is in the l_d phase, NMR diffusion could be used to confirm the presence of lipid rafts in a sample by measuring the presence of two populations with different diffusion coefficients.
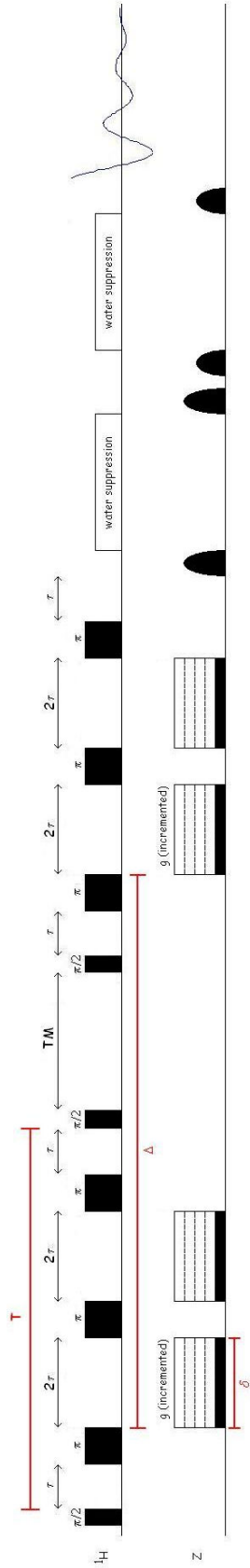
Figure 14: Pulse sequence for the stimulated echo experiment with separated gradients and water suppression
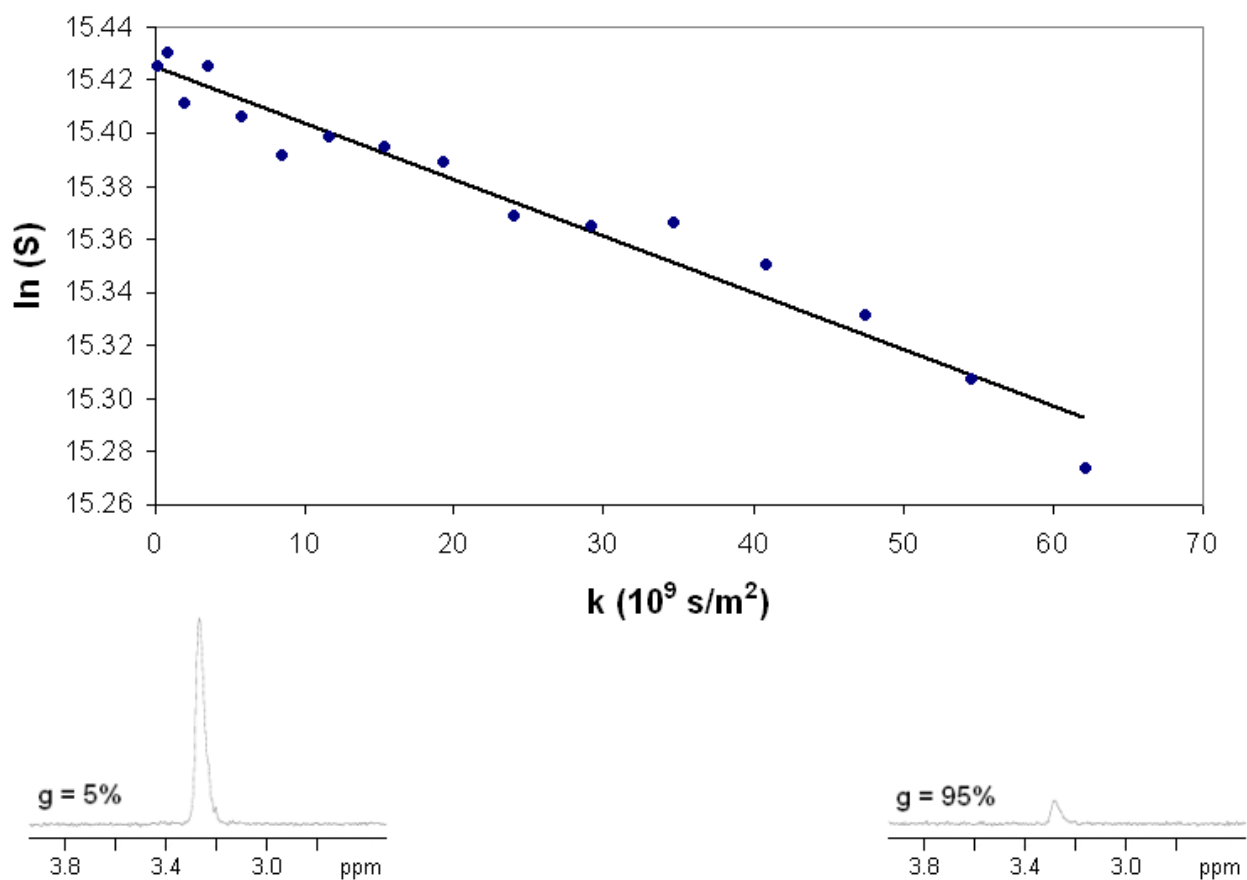
Figure 15: Plot of ln(S) vs. k for MLVs. Here, the absolute value of the slope of the line is the diffusion coefficient in m^2/s. Choline peaks from the ^{1}H NMR spectra of the first and last points are displayed below the plot.

3.5 - USING ATOMIC FORCE MICROSCOPY TO IMAGE PLANAR SUPPORTED BILAYERS

As stated previously, planar mica-supported bilayers have been shown to behave differently than free vesicles; specifically, the main phase transition is much broader and at a higher temperature than that of a free vesicle[4-6]. The atomic force microscope is well suited to detecting this effect, as the height change upon melting is easily observable. It should be noted, though, that this "decoupled leaflet melting" effect has only been observed on mica-supported bilayers; the effect has not yet been seen in a glass-supported bilayer.

If the surface-bottom leaflet interaction is indeed the nature of this effect, it is expected that the degree of decoupling will be less for a glass-supported bilayer than for a mica-supported one, owing to the lower surface charge of glass compared to mica[38,39]. If decoupled leaflet melting exists for glass-supported bilayers, it could be observed by repeatedly scanning the same area with the AFM at different temperatures. Charrier and Thibaudau continuously swept the temperature while scanning[5], but heating to a given temperature and imaging, then heating to a different temperature and imaging again should work equally well. The Spence research group has created a heating apparatus and insulated container for the AFM that is suitable to perform this experiment. This apparatus is capable of heating the planar supported bilayer to the desired temperature with stability better than 0.1 ℃ once equilibrated. A plot illustrating this is shown as Figure 16 (Courtesy Melissa Williams, Spence Group undergraduate).
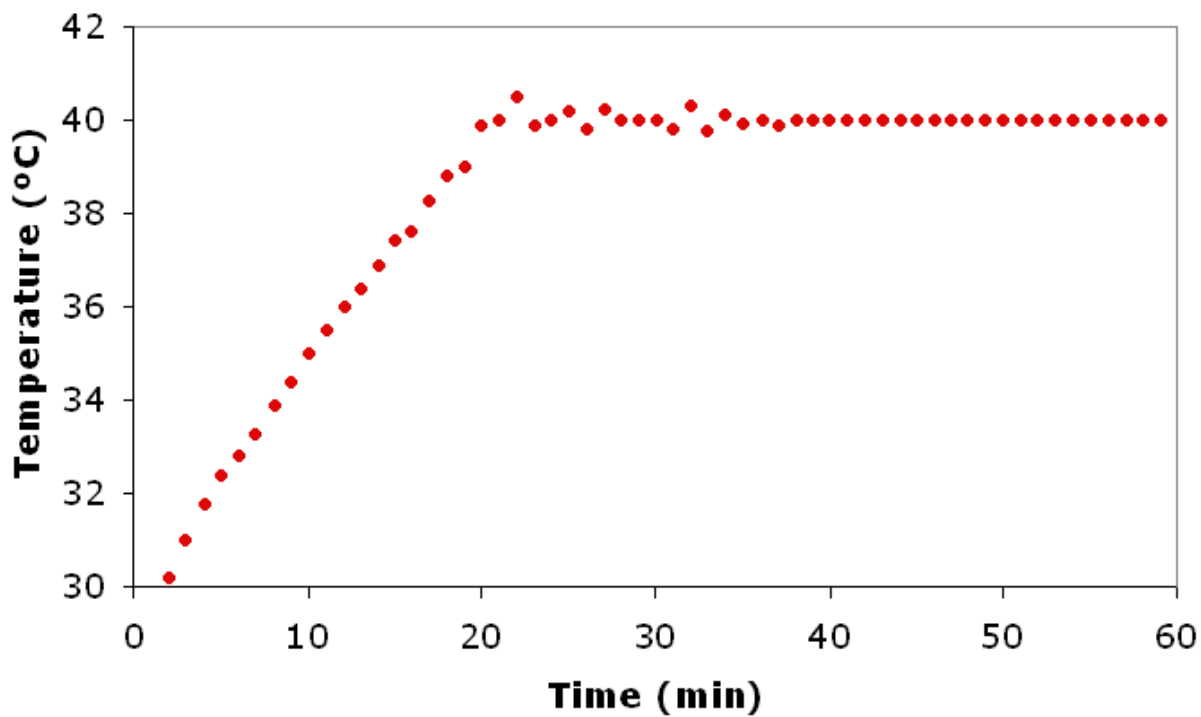
Figure 16: Temperature vs. time plot illustrating temperature stability of the AFM variable temperature control unit and insulated chamber. Courtesy Melissa Williams.

If decoupled leaflet melting is observed on glass, it is possible that the degree of decoupling can be tuned (i.e., a system can be made where the gap between top and bottom melting temperatures is adjustable). Holding to the hypothesis that the surface-bottom leaflet interaction is responsible for the behavior, the surface charge density of the support could conceivably be altered to yield a melting temperature gap of the desired width by changing in the pH of the buffer solution, surface functionalization[40-43], or electrochemical means. Such surface modification has been shown to alter the diffusion coefficient of a supported bilayer by as much as a factor of three[12], lending credence to the hypothesis that the degree of decoupling can also be controlled.

3.5.1 FUTURE AFM EXPERIMENTS

As stated above, the ultimate goal of this "AFM calorimetry" work is to observe decoupled leaflet melting in a glass-supported bilayer, or prove that the phenomenon does not exist for that system. Literature indicates that the experiment is straightforward. However, since it is hypothesized that the degree of decoupling will be less for glass than that of mica, care must be taken not to heat the sample too quickly, lest the two decoupled transitions coalesce into a single, broadened transition.

If decoupled leaflet melting is observed in glass-supported systems, it is conceivable that the degree of decoupling can be adjusted by making subtle changes to the surface chemistry of the solid support. If it is possible to tune the degree of decoupling in a planar supported bilayer, there may be applications that can exploit this to make useful devices.

4.0 - SUMMARY AND FUTURE EXPERIMENTS

4.1 - NMR SPECTROSCOPY OF SPHERICAL SUPPORTED BILAYERS

We have shown that complete spherical supported bilayers can be reliably created using standard techniques and methods, and that the product can be studied using ^{2}H static and ^{1}H MAS NMR.

^{2}H NMR spectra have been collected for DMPC-d_{54} SSBs and MLVs. The SSB and MLV ^{2}H NMR spectra are different, illustrating differences in structure (this is expected, and is presented here as a proof). A method to simulate ^{2}H NMR spectra and extract the order parameter profile has been developed exploiting the known angular distribution function of the spherical support. The simulation is capable of running on a regular computer (not a cluster) and does not take much time to run. A quickly prepared simulated ^{2}H NMR spectrum shows similarities to a published ^{2}H NMR spectrum of spherically oriented lipids; with more time spent fine-tuning the simulation, the order parameter profiles for our SSBs could be extracted. Following this, a lipid raft forming mixture will be analyzed using ^{2}H NMR spectroscopy, and the order parameter profile generating simulation.

An STE/WG sequence has been developed that enables measurement of diffusion coefficients for SSBs. This custom-written sequence allows observation of the desired slow-diffusing lipid signals while suppressing spurious solvent signals. This sequence has been employed to measure the diffusion coefficient of DMPC MLVs. Once all of the finer points of the experiment are perfected, it can be applied to measuring diffusion coefficients on SSBs.

4.2 - ATOMIC FORCE AND FLUORESCENCE MICROSCOPY OF PLANAR SUPPORTED BILAYERS

Supported planar bilayers have been imaged via atomic force microscopy. A method has been devised to determine whether a supported bilayer exists on a glass surface. The method exploits a tip-glass sticking interaction that is suppressed by the presence of a supported bilayer.

A temperature control device suitable for use with the AFM is in the final stages of testing. With this apparatus, it will be possible to observe the same area at various temperatures. It is hoped that the decoupled leaflet melting phenomenon will be observed for a glass-supported bilayer, and that the degree of decoupling can be adjusted by altering the surface chemistry of the support. Since it has been shown that the diffusion coefficient for a supported bilayer can be altered by changing the support surface chemistry[12], it is not unexpected that other properties can be changed as well.

4.3 - FURTHER FUTURE WORK – SUPPORTED MEMBRANE INTERRUPTIONS AND THEIR EFFECT ON LIPID RAFT FORMATION

It has been hypothesized that the reason lipid rafts are observed in model membranes but not in real cell membranes is that lipid raft formation is suppressed by disruptions to membrane structure, such as transmembrane and membrane-associated proteins often found in real cells. This hypothesis was tested by Yethiraj and Weisshaar[44] using a Monte Carlo simulation for a planar supported bilayer, both with and without non-lipid inclusions[44]. The simulation consisted of a 2D square lattice Ising model of a ternary lipid raft forming system, specifically, an equimolar mixture of palmitoyl-sphingomyelin, dioleoylphosphatidylcholine, and cholesterol. The experimentally determined phase transition temperature for this system is 40 ºC. The

simulation showed that the presence of static, non-lipid inclusions at area fractions as low as 10% depresses the order-disorder phase transition temperature by 35 ºC. If the ability of non-lipids to depress the melting temperature can be proved experimentally in a mixture of lipids known to be lipid raft forming under otherwise physiological conditions, it can be shown that lipid raft formation is inhibited in real cells.

Introducing these non-lipid interruptions can be done with the use of a small peptide. Gramicidin A has been shown to self-assemble across a supported lipid bilayer[45], is not prone to aggregation[35], and is commercially available. If introduced at low molarity to a supported bilayer, these peptides would provide the desired membrane interruptions, the effects of which could be observed using ^{2}H NMR or NMR diffusion (for spherical supported bilayers) or AFM (planar supports). If it is observed that lipid raft formation is inhibited in such systems, all of the mechanisms attributed to lipid rafts in real cells will need to be reevaluated.

5.0 REFERENCES

(1)   Brian, A. A.; McConnell, H. M. *Proc. Nat. Acad. Sci. USA* **1984**, *81*, 6159-63.

(2)   Schäfer, H.; Mädler, B.; Sternin, E. *Biophys. J.* **1998**, *74*, 1007-1014.

(3)   Heimburg, T. *Biochim. Biophys. Acta* **1998**, *1415*, 147-62.

(4)   Tokumasu, F.; Jin, A. J.; Feigenson, G. W.; Dvorak, J. A. *Ultramicroscopy* **2003**, *97*, 217-227.

(5)   Charrier, A.; Thibaudau, F. *Biophys. J.* **2005**, *89*, 1094-1101.

(6)   Yang, J.; Appleyard, J. *J. Phys. Chem. B* **2000**, *104*, 8097-8100.

(7)   Simons, K.; Ikonen, E. *Nature* **1997**, *387*, 569-572.

(8)   Stottrup, B. L.; Veatch, S. L.; Keller, S. L. *Biophys. J.* **2004**, *86*, 2942-2950.

(9)   Veatch, S. L.; Keller, S. L. *Phys. Rev. Lett.* **2002**, *89*, 268101.

(10)   Veatch, S. L.; Keller, S. L. *Biophys. J.* **2003**, *85*, 3074-83.

(11)   Veatch, S. L.; Polozov, I. V.; Gawrisch, K.; Keller, S. L. *Biophys. J.* **2004**, *86*, 2910-2922.

(12)   Seu, K. J.; Pandey, A. P.; Haque, F.; Proctor, E. A.; Ribbe, A. E.; Hovis, J. S. *Biophys. J.* **2007**, *92*, 2445-50.

(13)   Barenholz, Y.; Gibbes, D.; Litman, B. J.; Goll, J.; Thompson, T. E.; Carlson, F. D. *Biochemistry* **1977**, *16*, 2806-2810.

(14)   Stewart, J. C. M. *Anal. Biochem.* **1980**, *104*, 10-4.

(15)   Reimhult, E.; Höök, F.; Kasemo, B. *Langmuir* **2003**, *19*, 1681-91.

(16)   Bayerl, T. M.; Bloom, M. *Biophys. J.* **1990**, *58*, 357-62.

(17)   Johnson, S. J.; Bayerl, T. M.; McDermott, D. C.; Adam, G. W.; Rennie, A. R.; Thomas, R. K.; Sackmann, E. *Biophys. J.* **1991**, *59*, 289-94.

(18)   Daniel, S.; Albertorio, F.; Cremer, P. S. *MRS Bulletin* **2006**, *31*, 536-40.

(19)   Schönherr, H.; Johnson, J. M.; Lenz, P.; Frank, C. W.; Boxer, S. G. *Langmuir* **2004**, *20*, 11600-6.

(20)   Orädd, G.; Lindblom, G. *Magn. Reson. Chem.* **2004**, *42*, 123-131.

(21)   Köchy, T.; Bayerl, T. M. *Phys. Rev. E* **1993**, *47*, 2109-16

(22)   Bloom, M.; Davis, J. H.; MacKay, A. L. *Chem. Phys. Lett.* **1981**, *80*, 198-202.

(23)   Sternin, E.; Bloom, M.; MacKay, A. L. *J. Magn. Reson.* **1983**, *55*, 274-282.

(24)   Sternin, E.; Schäfer, H.; Polozov, I. V.; Gawrisch, K. *J. Magn. Reson.* **2001**, *149*, 110-113.

(25)   Levitt, M. H. *Spin Dynamics*; John Wiley & Sons: West Sussex, England, 2001.

(26)   Groves, J. T.; Ulman, N.; Boxer, S. G. *Science* **1997**, *275*, 651-653.

(27)   Lin, W.-C.; Blanchette, C. D.; Ratto, T. V.; Longo, M. L. *Biophys. J.* **2006**, *90*, 228-37.

(28)   Salafsky, J.; Groves, J. T.; Boxer, S. G. *Biochemistry* **1996**, *35*, 14773-81.

(29)   Cremer, P. S.; Boxer, S. G. *J. Phys. Chem. B* **1999**, *103*, 2554-9.

(30)   Hahn, E. L. *Phys. Rev.* **1950**, *80*, 580-94.

(31)   Tanner, J. E. *J. Chem. Phys.* **1970**, *52*, 2523-6.

(32)   Latour, L. L.; Li, L.; Sotak, C. H. *J. Magn. Reson. B* **1993**, *101*, 72-7.

(33)   Meiboom, S.; Gill, D. *Rev. Sci. Instrum.* **1958**, *29*, 688-91.

(34)   Gaede, H. C.; Gawrisch, K. *Biophys. J.* **2003**, *85*, 1734-1740.

(35)   Orädd, G.; Lindblom, G. *Biophys. J.* **2004**, *87*, 980-987.

(36)   Orädd, G.; Westerman, P. W.; Lindblom, G. *Biophys. J.* **2005**, *89*, 315-320.

(37)   Fordham, E. J.; Mitra, P. P.; Latour, L. L. *J. Magn. Reson. A* **1996**, *121*, 187-92.

(38)   Behrens, S. H.; Grier, D. G. *J. Chem. Phys.* **2001**, *115*, 6716-6721.

(39)   Heinz, W. F.; Hoh, J. H. *Biophys. J.* **1999**, *76*, 528-38.

(40)   Cha, T.; Guo, A.; Zhu, X.-Y. *Biophys. J.* **2006**, *90*, 1270-4.

(41)   Groves, J. T.; Ulman, N.; Cremer, P. S.; Boxer, S. G. *Langmuir* **1998**, *14*, 3347-50.

(42)   Kung, L. A.; Kam, L.; Hovis, J. S.; Boxer, S. G. *Langmuir* **2000**, *16*, 6773-6.

(43)   Schmitt, J.; Danner, B.; Bayerl, T. M. *Langmuir* **2001**, *17*, 244-6.

(44)   Yethiraj, A.; Weisshaar, J. C. *Biophys. J.* **2007**, biophysj.106.101931.

(45)   Ivanova, V. P.; Makarov, I. M.; Schaffer, T. E.; Heimburg, T. *Biophys. J.* **2003**, *84*, 2427-2439.